American Mineralogist, Volume 77, pages 221–224, 1992

LETTER

Scanning tunneling microscopy of pyrite {100}: Surface structure and step reconstruction

Carrick M. Eggleston
Institute for Water Resources and Water Pollution Control (EAWAG), Swiss Federal Institute of Technology, CH-8600 Dübendorf, Switzerland

Michael F. Hochella, Jr.
Department of Geology, Stanford University, Stanford, California 94305-2115, U.S.A.

Abstract

Scanning tunneling microscope (STM) images of atomically flat terraces on a pyrite (FeS_2) {100} surface are interpreted in terms of pyrite surface electronic structure; the electronic states at the top of the valence band, and therefore the states imaged in the STM under our conditions, are localized on Fe sites. The structure observed at a step differs from that of the terrace, probably because of band bending in response to electrostatic perturbations and shifting of atomic positions at the step edge; convolution of atomic and electronic structure information in STM images precludes unequivocal interpretation of step structure. Nevertheless, the images suggest that steps may provide paths of enhanced conductivity, which could affect pyrite surface redox reactivity.

Introduction

Pyrite (FeS_2), the most common sulfide mineral, is an important geochemical redox and photoredox reactant (e.g., Waite, 1990). Oxidation of pyrite and other sulfide minerals is of importance in processes ranging from acid mine drainage and ore processing (Biegler and Swift, 1979; Nordstrom, 1982; McKibben and Barnes, 1986) to scavenging of precious metal complexes during ore formation (Bakken et al., 1989; Bancroft and Hyland, 1990; Eggleston and Hochella, 1991). Pyrite and other transition-metal dichalcogenides are also important electrochemical regenerative and photoelectrolysis-cell electrodes (Ennaoui et al., 1986; Fan and Bard, 1991). Consequently, pyrite bulk and surface electronic structure have been studied (e.g., Li et al., 1974; Jaegermann and Tributsch, 1988). Scanning tunneling microscopy (STM), which allows atomic-resolution imaging of surface electronic state distribution, has also been applied to pyrite surfaces. Eggleston and Hochella (1990) imaged Fe sites on a fresh pyrite {101} surface; Fan and Bard (1991) imaged a mixture of Fe and S states and used tunneling spectroscopy to probe surface electronic structure.

In this letter, we present and interpret STM images of a pyrite {100} surface. The results are in general agreement with previous molecular orbital (MO) and UV photoelectron spectroscopy (UPS) results, but the electronic (and perhaps atomic) structure near step edges is perturbed. Steps impose an altered electrostatic and bonding environment that apparently causes a slightly different set of states to be imaged near steps relative to terraces. These observations have implications for pyrite surface redox reactivity.

Experimental data

Natural pyrite specimens (from an unknown locality) were obtained from the Stanford Mineral Collection. The pyrite bulk band gap is approximately 0.9 eV (Ferrer et al., 1990). Crystals were fractured and imaged in polyphenyl ether, a nonconductive and nonreactive oil that has been used in previous studies of sulfide surfaces and which inhibits reaction of the surface with air (Eggleston and Hochella, 1991). Although pyrite does not have a well-developed direction of cleavage, fracture surfaces that appeared parallel to a {100} face were selected for imaging.

We used a Digital Instruments Nanoscope II STM; STM operation has been described elsewhere (e.g., Hochella, 1990; Avouris, 1990). Briefly, a sharp metal tip is piezoelectrically rastered over the surface, sufficiently close for overlap of tip and surface electronic states. This allows a small net current (I_T) to flow, by means of quantum mechanical tunneling, in response to a bias voltage applied to the sample (V_S). With a sufficiently sharp tip, atomic resolution may be achieved. Specific imaging conditions are given in the figure captions.

Results and discussion

Figure 1 shows an STM image of pyrite taken at −40 mV V_S. Under these conditions, electrons tunnel from occupied states at the top of the valence band (VB) to

0003–004X/92/0102–0221$02.00

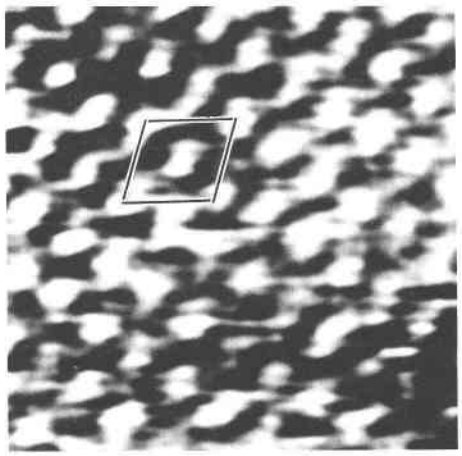

Fig. 1. STM image taken in the constant-current mode (contrast results from variation in tip height) at −40.1 mV and 1.2 nA. The image area is 31 by 31 Å, and total relief is approximately 0.5 Å. A surface unit cell for pyrite (100) is drawn in, allowing for drift, with Fe-localized states at the corners (see text). The image is low-pass filtered to remove high frequency noise.

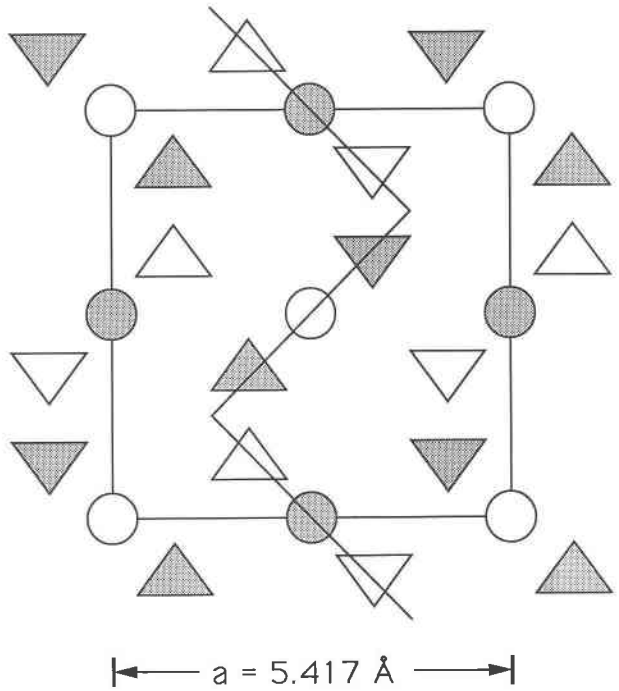

Fig. 2. Projection of the pyrite structure on the (100) plane (modified from Fan and Bard, 1991), showing a zigzag path (see Fig. 4 and text). Open circles designate top layer Fe positions; shaded circles designate second layer Fe positions; open triangles pointing up designate S sites just above the top Fe layer, open triangles pointing down designate S sites just below top Fe layer (distance above or below layer = $0.115a$); shaded triangles occupy sites analogous to the unshaded triangles, except above and below second layer Fe. The S-S bond of first-layer S_2 pairs crosses the midpoints of the cell edges.

unoccupied conduction band (CB) states on the tip. Figure 2 shows a projection of the pyrite structure on (001). Note that thermal and piezoelectric drift (which causes nonorthogonal tip rastering) was substantial during imaging in Figure 1, which caused distortion of the square-surface unit cell. Nevertheless, comparison of the arrangement and density of peaks observed in Figure 1 with the arrangement of equivalent Fe and S sites in Figure 2 allows two possibilities: either the peaks in Figure 1 correspond to Fe sites and S sites are not imaged, or S-S pairs are imaged as a single site and Fe sites are not imaged. In order to interpret Figure 1, we briefly discuss pyrite surface electronic structure.

The MO calculations of Vaughan et al. (1974) and Li et al. (1974) for Fe-S clusters suggest that states at the top of the VB are Fe 3d-like (t_{2g}) states localized on Fe sites. Figure 3A summarizes the results of Li et al. (1974) for a combined MO and UPS study of pyrite. The UPS data show a narrow peak at the top of the VB whose relative intensity increases with UV energy, as expected for localized d-like states and in agreement with the MO calculations. At a surface, the symmetry which causes degeneracy of t_{2g} states in the bulk is broken; this may be thought of as less crystal field stabilization of the d_{xy} orbital relative to that of the d_{xz} and d_{yz} orbitals because of the missing ligand at the surface (Jaegermann and Tributsch, 1988; Waite, 1990). This effect is illustrated in Figure 3B; the nondegenerate peaks are probably too close together to be resolved in the UPS spectrum of Figure 3A. Thus, the states at the top of the surface VB probably correspond to Fe 3d-like dangling bond surface states.

The above arguments apply in a vacuum, but the situation may be different for a surface fractured under oil, to which species may chemisorb. Recoordination of surface Fe sites by adsorbates would serve to stabilize the dangling bond states (i.e., shift electron density deeper into the VB) but would probably not entirely restore the bulk symmetry that allows t_{2g} state degeneracy (see Jaegermann and Tributsch, 1988). Thus, although chemisorption (in this case, probably weak bonding of oil molecules) might alter the exact energy of the surface states, the overall interpretation still stands, except that the surface states would not be referred to as dangling bonds. This interpretation is supported by the fact that tunneling spectra taken in air by Fan and Bard (1991) show that the observed state density near the Fermi level (E_F) agrees with the MO and UPS results.

The above discussion suggests that the states we image as bright spots (points of high tunneling current) in Figure 1 are most likely localized Fe 3d states at the surface. Based on this interpretation, a surface unit cell is drawn in Figure 1 that corresponds to the cell shown in Figure 2. This interpretation is similar to that offered by Fan and Bard (1991) for their STM images, except that imaging was done in air and thus differs slightly from ours (see below).

Figure 4 shows a step only a few nanometers away from the area imaged in Figure 1. The step is parallel to [010],

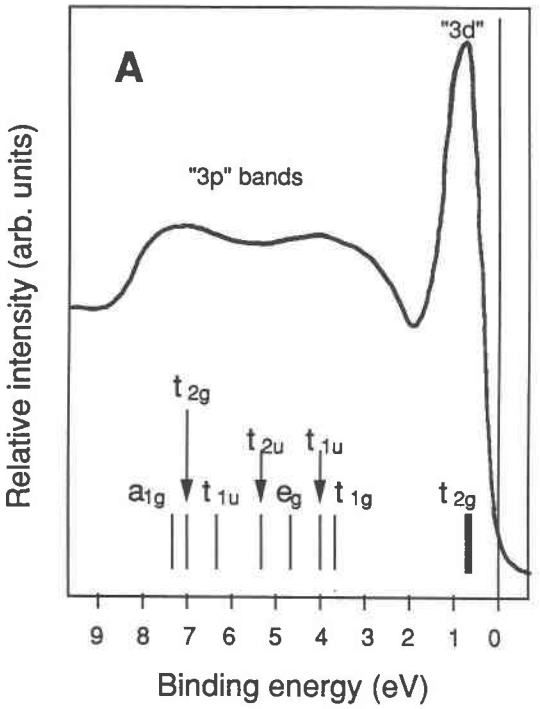

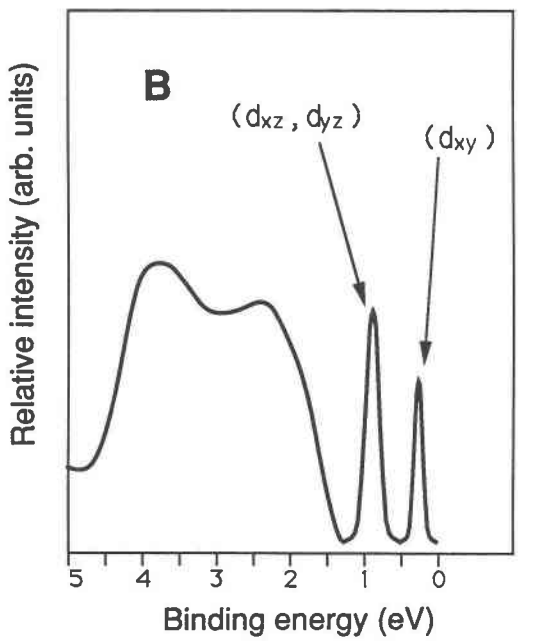

Fig. 3. (A) UPS spectrum from Li et al. (1974) for pyrite, for UV energy of 30 eV. Also plotted are energy levels from their MO calculations and band assignments. The "3p" bands contain states that have mixed 3p and 3d character resulting from bonding interactions. (B) Schematic illustration of surface states for pyrite {100}, based on Jaegermann and Tributsch (1988). A hypothetical spectrum is plotted, showing states that might be observed at a surface for a spectrometer with near-perfect energy resolution. Asymmetry at the surface breaks the Fe 3d t_{2g} state degeneracy, giving two surface states.

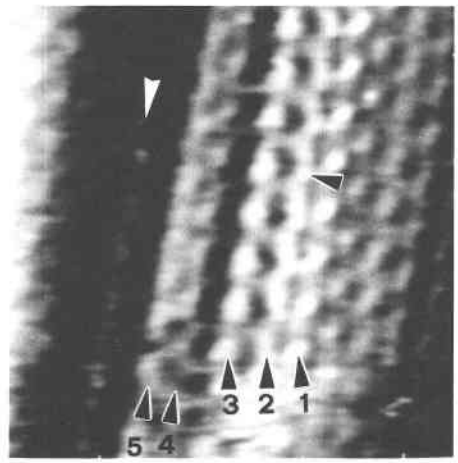

Fig. 4. STM image at 44 × 44 Å of a step taken under the same conditions as Figure 1. Atomic rows near the step edge with perturbed electronic and atomic structure are labeled with numbers and arrows and discussed in the text. The blurred area in the lower part of the image may be due to adsorbate interference with tunneling. The image is low-pass filtered to remove high frequency noise.

and steps down from right to left; the step height (measured from the highest point on row 3 to the lowest point to the left) is 2.8 Å, which is within error (ca. 10%) of half a pyrite unit-cell edge (5.42 Å). Clearly, however, the structure observed along the step differs from that of the terrace (Fig. 1). Approaching the step from the right in Figure 4, we see that rows 1–3 are brighter than rows on the terrace and that row 2 appears as a zigzag chain rather than as a row of distinct spots.

Fe atoms on a terrace have one dangling bond; at a step, Fe sites with two dangling bonds may occur. That could increase the state density at step sites, making them appear bright relative to terrace sites. However, Figure 4 does not support this argument because sites not at the step edge also appear relatively bright. A second possibility is that coordination undersaturation of step sites (or, given chemisorption, coordination asymmetry) results in site potentials at steps that differ from those of terraces. Different site potentials would cause slight band bending (Zangwill, 1988), i.e., alteration of the energies of occupied states relative to those on the terrace, creating step states, just as surfaces have surface states not found in the bulk. The distribution of such step states would not be restricted to atoms at the step edge but might extend several atoms away from the step edge and thus affect the relative brightness of nonstep sites in an STM image, as observed. For example, the site marked with an unlabeled black arrow in Figure 4 (in the zigzag chain) does not correspond to an Fe site; by comparison to Figure 2, it corresponds more closely to an S site. This could result if, because of band bending, contributions to the tunneling current are made from occupied states lower in the VB (which have some S character; see Waite, 1990; Li et al., 1974). Indeed, Fan and Bard (1991) attributed

zigzag features in their STM images of terraces (they did not image steps at high resolution) to contributions from S states. However, this does not explain why only S sites in row 2 are imaged.

A third possibility is that variation in site brightness is at least partially caused by relaxation or reconstruction of atomic positions near steps; for example, perhaps S atoms in row 2 are higher than those in other rows. Similarly, Fe sites near the step appear either to be higher than on the terrace or to have localized states that are slightly destabilized in energy; we cannot distinguish between these possibilities. The irregular spacing of rows near the step (e.g., the gap between rows 3 and 4) may indicate a shift in atomic positions near the step, but it may also be argued that the rows left of row 3 (rows 4, 5, and the faint row marked by a white arrow) correspond to shifts in electronic or atomic structure on the lower terrace and that row 3 is the step edge. Thus, although Figure 4 probably reflects significant shifts of both electronic and atomic structure near steps relative to terraces, the convolution of electronic structure and atomic position information in STM images does not allow a single step structure model to be proved (e.g., see Becker and Vickers, 1990).

Conclusions

Despite the difficulties discussed above, Figure 4 is qualitatively consistent with perturbations of electronic structure near steps (i.e., the creation of step states), probably combined with shifts in atomic positions near steps. Such atomic and electronic structure perturbations probably affect the reactivity of step sites relative to terrace sites. For example, electron transfer from the highest occupied molecular orbitals (HOMOs) of S_2 to an oxidant was proposed by Luther (1990) in a frontier molecular orbital approach to pyrite oxidation. This study and that of Li et al. (1974) show that the HOMOs (strictly speaking, bands) for fresh pyrite {100} terraces are localized on Fe; however, species (O_2, H_2O, etc.) chemisorbed from air and perturbations at steps may alter this situation, resulting in states with S character at the top of the VB. Indeed, the images of Fan and Bard (1991) for a terrace in air show states with S character, as does our image of a step. It is interesting to speculate that the states imaged in STM correspond to reactive frontier bands whose characteristics depend on the local structure (e.g., steps) and the identity of adsorbates.

Steps, by means of step states, may thus provide pathways for enhanced conductivity and redox reactivity relative to bulk or terrace sites. Such conclusions are not surprising; steps are generally thought to be relatively reactive. However, we may now begin to examine the microscopic physical and electronic basis for enhanced reactivity, which may ultimately lead to a better understanding of surface reaction mechanisms.

Acknowledgments

We thank George Parks and Pat Johnsson (Stanford), Virgil Elings (Digital Instruments), and an anonymous reviewer for useful discussions and comments. This research was supported by the Petroleum Research Fund (American Chemical Society grant PRF 22892-ACS,2) and the National Science Foundation (EAR-9105000), both to M.F.H.

References cited

Avouris, Ph. (1990) Atom-resolved surface chemistry using the scanning tunneling microscope. Journal of Physical Chemistry, 94, 2246–2256.

Bakken, B.M., Hochella, M.F., Jr., Marshall, A.F., and Turner, A.M. (1989) High resolution microscopy of gold in unoxidized ore from the Carlin mine, Nevada. Economic Geology, 84, 171–179.

Bancroft, G.M., and Hyland, M.M. (1990) Spectroscopic studies of adsorption/reduction reactions of aqueous metal complexes on sulphide surfaces. In Mineralogical Society of America Reviews in Mineralogy, 23, 511–558.

Becker, R., and Vickers, J. (1990) Determination of surface atomic positions by scanning tunneling microscope observations. Journal of Vacuum Science and Technology, A8 (1), 226–232.

Biegler, T., and Swift, D.A. (1979) Anodic behavior of pyrite in acid solutions. Electrochimica Acta, 24, 415–420.

Eggleston, C.M., and Hochella, M.F., Jr. (1990) Scanning tunneling microscopy of sulfide surfaces. Geochimica et Cosmochimica Acta, 54, 1511–1517.

——— (1991) Scanning tunneling microscopy of galena (100) surface oxidation and sorption of aqueous gold. Science, 254, 983–986.

Ennaoui, A., Fiechter, S., Jaegermann, W., and Tributsch, H. (1986) Photoelectrochemistry of highly quantum efficient single-crystalline n-FeS_2 (pyrite). Journal of the Electrochemical Society, 133, 97–106.

Fan, F.R., and Bard, A.J. (1991) Scanning tunneling microscopy and tunneling spectroscopy of n-type iron pyrite (n-FeS_2) single crystals. Journal of Physical Chemistry, 95, 1969–1976.

Ferrer, I.J., Nevskaia, D.M., Heras, C., and Sanchez, C. (1990) About the band gap nature of FeS_2 as determined from optical and photoelectrochemical measurements. Solid State Communications, 74 (9), 913–916.

Hochella, M.F., Jr. (1990) Atomic structure, microtopography, composition, and reactivity of mineral surfaces. In Mineralogical Society of America Reviews in Mineralogy, 23, 87–132.

Jaegermann, W., and Tributsch, H. (1988) Interfacial properties of semiconducting transition metal chalcogenides. Progress in Surface Science, 29, 1–167.

Li, E.K., Johnson, K. H., Eastman, D.E., and Freeouf, J.L. (1974) Localized and bandlike valence-electron states in FeS_2 and NiS_2. Physical Review Letters, 32 (9), 470–472.

Luther, G.W. (1990) The frontier-molecular-orbital theory approach in geochemical processes. In W. Stumm, Ed., Aquatic chemical kinetics, p. 173–198. Wiley, New York.

McKibben, M.A., and Barnes, H.L. (1986) Oxidation of pyrite in low temperature acidic solutions: Rate laws and surface textures. Geochimica et Cosmochimica Acta, 50, 1509–1520.

Nordstrom, D.K. (1982) Acid sulfate weathering. Special Publication 10, 37 p. Soil Science Society of America, Madison, Wisconsin.

Vaughan, D.J., Tossell, J.A., and Johnson, K.H. (1974) The bonding of ferrous iron to sulfur and oxygen in tetrahedral coordination: A comparative study using SCF $X\alpha$ scattered wave molecular orbital calculations. Geochimica et Cosmochimica Acta, 38, 993–1005.

Waite, T.D. (1990) Photo-redox processes at the mineral-water interface. In Mineralogical Society of America Reviews in Mineralogy, 23, 559–603.

Zangwill, A. (1988) Physics and surfaces, 454 p. Cambridge University Press, Cambridge, U.K.

Manuscript received November 8, 1991
Manuscript accepted December 4, 1991